arXiv:1403.4790v1 [cond-mat.mes-hall] 19 Mar 2014

Group-velocity slowdown in quantum-dots and quantum-dot molecules

Stephan Michael,[1] Weng W. Chow,[2] and Hans Christian Schneider[1]

[1]*Department of Physics and Research Center OPTIMAS, University of Kaiserslautern, P.O. Box 3049, 67653 Kaiserslautern, Germany*

[2]*Semiconductor Materials and Device Sciences Department, Sandia National Laboratories, Albuquerque, NM 87185-1086, USA*

Abstract

We investigate theoretically the slowdown of optical pulses due to quantum-coherence effects in InGaAs-based quantum dots and quantum dot molecules. Simple models for the electronic structure of quantum dots and, in particular, quantum-dot molecules are described and calibrated using numerical simulations. It is shown how these models can be used to design optimized quantum-dot molecules for quantum coherence applications. The wave functions and energies obtained from the optimizations are used as input for a microscopic calculation of the quantum-dot material dynamics including carrier scattering and polarization dephasing. The achievable group velocity slowdown in quantum-coherence V schemes consisting of quantum-dot molecule states is shown to be substantially higher than what is achievable from similar transitions in typical InGaAs-based single quantum dots.

I. INTRODUCTION

Quantum coherence effects arise from interference in the transition amplitudes between quantum states in the presence of a coherent light field.[1–6] Perhaps the best known of these effects are electromagnetically induced transparency (EIT) or slow light. For many years, there have been proposals to realize quantum coherence effects in few-level systems in solids[7–14] and, in particular, in semiconductors.[7,9,10,15–20] Slow light has been achieved in semiconductor quantum wells (QWs) with coherent population oscillations of excitons.[11,21] Other approaches inlcude slow light in photonic crystals.[22]

Semiconductor QDs exhibit electron and hole states with discrete energies, and are reminiscent of atomic few-level systems.[23–25]. The dephasing of the quantum coherences, however, is much different from atomic systems. In particular, electron-hole transitions in semiconductors typically have short dephasing times which are detrimental for quantum coherence effects and limit the achievable group velocity slowdown, even in QDs,[26–29]. Depending on the levels that are connected by drive and probe fields, Λ, V and ladder schemes can be realized.[1] A direct comparison of these different setups in the framework of an atomic-like model with dephasing constants points toward the V scheme as being the most useful and optimizable setup for group-velocity reduction.[26]

The reason for investigating V type schemes instead of the Λ schemes treated in earlier papers of us[24,28,29] is that in Λ scheme the quantum coherence connects two hole states. The hole states in GaAs-based semiconductor QDs are generally closely spaced and the electron-phonon interaction with polaronic broadening efficiently couples them and leads to a pronounced dephasing for coherences involving hole states. Because the drive or probe (electron-hole) polarization is susceptible to the same dominant hole contributions of the dephasing, the dephasing of the probe and quantum coherence are roughly of equal size, which is not a good condition for quantum coherence effects. In this case, no group-velocity slowdown can be achieved with a CW drive pulse. Instead, a short drive pulse is necessary to slow down the probe pulse,[28,29] but the time window during which the probe pulse is slowed down, is quite short.[30]

The present paper analyzes V-type quantum coherence schemes in the framework of a microscopic model, both for QDs and QD molecules. It is a companion to our recent paper[31], in which we showed theoretically that one can achieve slowdown of optical pulses in InGaAs-

based QD molecules that is much larger than in V-type coherence schemes for single QDs systems. As explained in Ref. 31, both the single QD and QD molecule V schemes perform better than the Λ schemes analyzed in our earlier studies[28,29], because the dephasing rates for the probe and quantum coherence are significantly different in Λ and V schemes. The encouraging results for the achievable group velocity slowdown in QD molecules contained in Ref. 31 are based on an optimized design for the QD molecule states that leads to a long lived coherence between two electronic levels used in the quantum coherence schemes.

In this paper, we give more details about the "optimization" of the QD and QD molecule structures used as input for the microscopic calculation of scattering and dephasing contributions for polarization (and level population). A detailed description of the scattering and dephasing contributions in quantum coherence V schemes is contained in Ref. 31, here we focus on the modeling of the electronic structure of QDs and QD molecules to maximize the achievable slowdown. We describe comparatively simple models for the QD states, which can be calibrated by more realistic numerical calculations, but also permit us to vary important properties of the QD states by changing one (or a few) meaningful parameters, such as the depth of the QD confinement potential and/or the distance between the QDs making up the QD molecule. For the optimization of the QD structures, the figure of merit is a quasi-equilibrium slow-down factor determined by its group-velocity reduction in the frequency domain. The slow down factor is calculated using a microscopic many-particle approach including carrier scattering and polarization dephasing.

The paper is organized as follows. In Section II we give a brief review over the theory of semiconductor material dynamics, i.e. the semiconductor Bloch equations. Section III is devoted to single quantum dots, and investigates the influence of the confinement potential and the lattice temperature on achievable slowdown for InGaAs single QDs. Section IV is concerned with QD molecules. Here, we describe our model for QD molecules and show in some detail how to compute the electronic energies and states, and highlight the features of our optimized QD molecule for group-velocity slowdown. The results for group-velocity slowdown are compared with those of single QDs.

II. SEMICONDUCTOR BLOCH EQUATIONS

In this section, we review the theory of semiconductor material dynamics, which is necessary to describe the V-scheme of the QD system. First of all, we introduce the optical field written in the form

$$\vec{E}(t) = \frac{1}{2}\hat{x}[\mathcal{E}(t)e^{-i\omega t} + \mathcal{E}(t)e^{i\omega t}] \tag{1}$$

where $\hat{x}$ is the polarization unit vector in x direction, and ω is the frequency of the field $\vec{E}$. The corresponding macroscopic polarization has the form

$$\vec{P}(t) = \frac{1}{2}\hat{x}[\mathcal{P}(t)e^{-i\omega t} + \mathcal{P}^*(t)e^{i\omega t}] \tag{2}$$

where $\mathcal{P}$ is the complex slowly varying envelope. The macroscopic polarization P is connected with the microscopic polarization by

$$P = \frac{N_d}{L}\sum_{\alpha,\beta}\mu_{\alpha\beta}p_{\alpha\beta} + c.c. \tag{3}$$

where N_d is the in-plane density of the QDs, L is the thickness of the region, in which the QD layer is embedded, $\mu_{\alpha\beta}$ are the dipole matrix elements and the summation index α or β refers to QD system electron or hole states, respectively.

The dynamics of the polarizations and carrier distributions at the single-particle level are calculated in the framework of the semiconductor Bloch equations for the reduced single-particle density matrix. We denote in the following electron and hole levels in the QD α and β, respectively. For the V system of interest in this paper one obtains the following equations of motion for the "interband" polarizations, $p_{\alpha\beta}$, and the "intra(electron-)band" polarizations $p_{\alpha'\alpha''}$

$$\frac{\partial}{\partial t}p_{\beta\alpha} = -i\omega_{\alpha\beta}p_{\beta\alpha} - i\Omega_{\alpha\beta}\left(n^c_\alpha - n^v_\beta\right) - i\sum_{\alpha'\neq\alpha}\Omega_{\alpha'\beta}p_{\alpha'\alpha} + S_{\beta\alpha} \tag{4}$$

$$\frac{\partial}{\partial t}p_{\alpha'\alpha''} = -i\omega_{\alpha''\alpha'}p_{\alpha'\alpha''} - i\Omega_{\alpha''\alpha'}\left(n^c_{\alpha''} - n^c_{\alpha'}\right) + i\sum_{\beta'}\left(\Omega_{\alpha''\beta'}p_{\alpha'\beta'} - \Omega_{\beta'\alpha'}p_{\beta'\alpha''}\right) + S_{\alpha'\alpha''} \tag{5}$$

In particular, the polarization $p_{e_0e_1}$ here is the *quantum coherence*. For the time evolution of the conduction and valence band populations, n^c_α and n^v_β, one obtains

$$\frac{\partial}{\partial t}n^c_\alpha = i\sum_{\beta'}\left(\Omega_{\alpha\beta'}p_{\alpha\beta'} - \Omega_{\beta'\alpha}p_{\beta'\alpha}\right) + S_{\alpha\alpha} \tag{6}$$

$$\frac{\partial}{\partial t}n^v_\beta = i\sum_{\alpha'}\left(\Omega_{\beta\alpha'}p_{\beta\alpha'} - \Omega_{\alpha'\beta}p_{\alpha'\beta}\right) + S_{\beta\beta} \tag{7}$$

The coherent contributions of the above equations contains transition frequencies $\omega_{\alpha\beta}$ and renormalized Rabi frequencies $\Omega_{\alpha\beta} = \hbar^{-1}\mu_{\alpha\beta}E(t) + \Omega_{\alpha\beta}^{\mathrm{HF}}$ with $E(t) = \frac{\mathcal{E}(t)}{2}[e^{-i\omega t} + e^{i\omega t}]$ are renormalized by excitation-dependent Hartree-Fock (HF) contributions resulting from the Coulomb interaction, as discussed, e.g., in Refs. 24, 28, and 29. The correlation contributions are generally denoted by S and contain the influence of carrier-carrier and carrier-phonon interactions beyond the Hartree-Fock level. In particular, $S_{\alpha,\alpha}$ and $S_{\beta,\beta}$ describe scattering contributions in the dynamical equations for the electron and hole distributions as well as dephasing $S_{\beta\alpha}$, $S_{\alpha'\alpha''}$ in the dynamical equations for the coherences. The correlation contributions S are derived and the explicit equations are given in Ref. 31.

For the calculation of the implied Coulomb matrix elements and carrier-phonon interaction matrix elements in the dots-in-a-well system, QD and QW states has to be considered. Our approach can not handle the whole dots-in-a-well system in one "box". Such an approach would naturally yield localized and delocalized eigenfunctions that are orthogonal to each other. We have to treat the calculation of the three-dimensional QD states separately from the calculation of the QW states. To describe the combined system we orthogonalize the QW states to the QD states as described in Ref. 32. The outcome of this are localized and delocalized eigenfunctions that are orthogonal to each other as used in Ref. 31.

To determine the spectral gain and group-velocity slowdown in a V-system, we solve the dynamical equations (4)–(7) for a strong cw drive field with fixed angular frequency ω_d and a weak cw probe field with angular frequency ω_p. From the steady-state value of the polarization $\mathcal{P}$ we determine the gain via

$$g(\omega_p) = -\frac{\omega_p}{2\varepsilon_0 c n_b \mathcal{E}_p}\Im[\mathcal{P}] \tag{8}$$

and refractive-index change

$$\delta n(\omega_p) = -\frac{1}{2\varepsilon_0 n_b \mathcal{E}_p}\Re[\mathcal{P}] \tag{9}$$

where n_b is the background refractive index of the host material. The group-velocity slowdown factor is defined by $S(\omega_p) = n_b + \omega_p \frac{d(\delta n)}{d\omega_p} \equiv n_b + S'(\omega_p)$, but we will consider only the contribution from the index change

$$S'(\omega_p) = \omega_p \frac{d(\delta n)}{d\omega_p} \tag{10}$$

in order to remove the static contribution, which describes the change in group velocity due to the background refractive index as compared to vacuum.

III. SINGLE QUANTUM DOTS

In this section we calculate the group-velocity slowdown for single QDs with a V-type configuration of probe and drive pulses, see Figure 1(b) for a sketch of the resulting band lineup. The results of this Section make use of a simplified QD model in order to show– including a microscopic calculation of the relevant dephasing of the quantum coherences– the possibility of group velocity slowdown with a CW drive. These results are also used as a baseline to measure the improvements for group-velocity reduction that come from using optimized QD molecules, which will be discussed in the next section.

We describe briefly the simple QD model used in this section to calculate the matrix elements needed for the calculation of the microscopic QD dynamics described in Section II. We assume that the QDs are contained in a surrounding quantum well, and that the envelope function for electron and hole states can be written as a product of a wave function in the growth direction z of the QW and an in-plane part

$$\Phi_{\mathrm{3D}}(r,\varphi,z) = N\,\Phi_{\parallel}(r,\varphi)\Phi_{\perp}(z) \tag{11}$$

where N is a normalization constant. The in-plane confinement potential is assumed to be harmonic and is completely specified by the harmonic oscillator level spacing $\hbar\omega_{\mathrm{HO}}$, which is chosen in accordance with measured/calculated values. The in-plane part of the wave function is then given by eigenfunctions of the two-dimensional harmonic oscillator, cf. Ref.[32,33] The band lineup of the QD in this simple model is therefore defined by the spacing of electron and hole levels, as well as the fundamental band-gap.

In the following we use the QD model described above to define two different QDs and investigate the group-velocity slowdown performance of these QDs by calculating the spectral gain and group-velocity slowdown from the QD material dynamics described in section II. In particular, we compare the results of the slowdown factor for different lattice temperatures and cw drive intensities.

The V-scheme employed here is shown schematically in figure 1. We assume an ensemble of InAs QDs embedded in a GaAs QW with a width of 16 nm. We will investigate a shallow and a deep QD with three confined electron and hole states. Thus we have one doubly degenerate excited state and one ground state with the energy values in Table I. Using an analytical model only diagonal transitions are dipole allowed because of symmetry

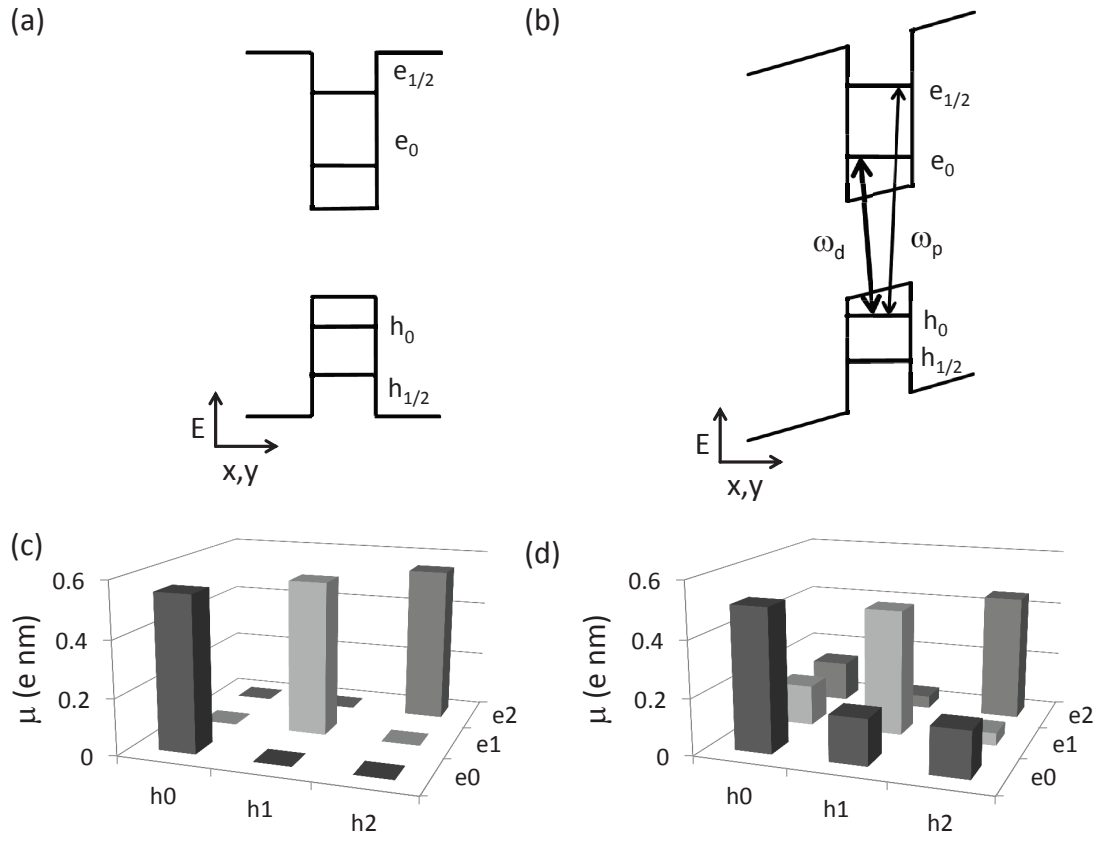

FIG. 1. Energy spectrum and setup of the cw drive and probe fields for the slowing down of the probe field in a V-scheme with (a) and without (b) static electric field. Dipole interband matrix elements μ for a deep QD with (c) and without (d) static electric field. The static field makes the V-scheme possible because it breaks the symmetry responsible for the vanishing of the off-diagonal dipole matrix elements.

considerations. However, to realize a V-scheme one needs off-diagonal interband transitions. We achieve this by including a symmetry breaking static electric field. To make off-diagonal dipole matrix elements appreciable, we use an external electric field in the plane of the QW with a field strength of 4.0 mV nm^{-1} for the deep QD. The diagonal and off-diagonal dipole moments with and without the external electric field are shown in figure 1. The dipole matrix elements make a V-scheme with a drive-pulse between the electron and hole ground state and a probe-pulse between the hole ground and the excited electron states possible. The quantum coherence of the V scheme is between the electron ground and the excited electron states. The energy gap between the electron and hole ground state is taken to be

Shallow Dot			Deep Dot		
	E_e (meV)	E_h (meV)		E_e (meV)	E_h (meV)
e/h_0	-70	30	e/h_0	-150	50
$e/h_{1/2}$	-30	15	$e/h_{1/2}$	-60	20

TABLE I. Electron (e) and hole (h) energies of single-particle states in the single QDs.

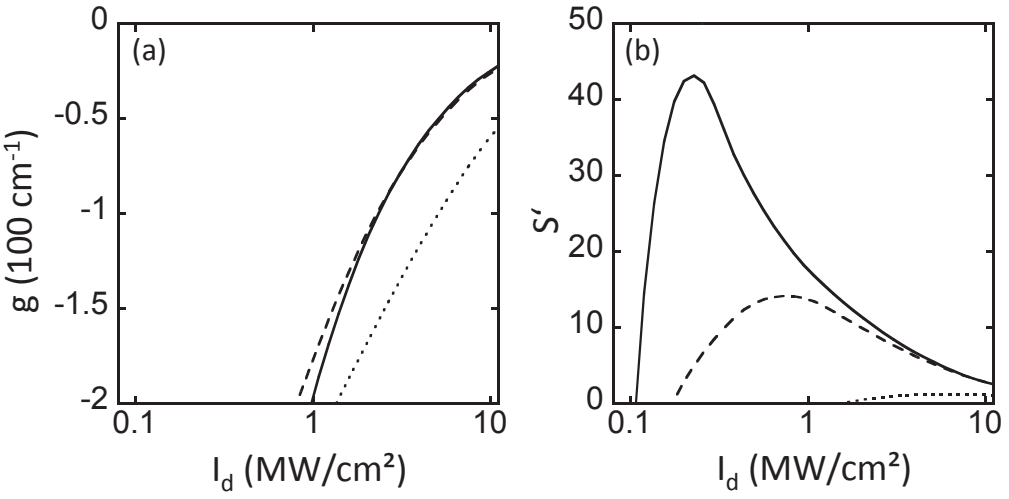

FIG. 2. Peak gain (a) and peak slowdown (b) versus drive intensity for a shallow (dotted line) and a deep (solid and dashed line) QD. The lattice temperature is 150 K (solid line) and 300 K (dashed and dotted line).

around 1.2 eV.

We compare a shallow and a deep QD for slow light applications in figure 2. We choose a weak cw probe with intensity 45 W/cm^2. For a given cw drive intensity the spectral gain and group-velocity slowdown can be determined as described in section II by running the calculation until a steady state for the probe polarization is reached. Afterwards the peak gain and peak slowdown versus cw drive intensity can be plotted as shown in figure 2.

First, we discuss the shallow and deep QD results for a lattice temperature of 300 K. Below a drive intensity of 0.1 MW/cm^2 we find a significant peak absorption without peak slow-down for both QDs. Above a drive intensity of 0.1 MW/cm^2 the peak slow-down factor for similar peak absorption values is higher for the deep QD. A optimum drive intensity

around 1.0 MW/cm^2 facilitate only a small absorption and a significant peak slowdown for the probe of the deep QD. For the shallow QD no significant peak slowdown is reached. Therefore, a maximum of slowdown with a minimum of absorption is accomplished better for the deep QD as for the shallow QD. The results can be explained in the following way: If we want to reach transparency with an appreciable slowdown, the dephasing rate of the polarization from the cw probe has to significantly exceed the dephasing rate of the quantum coherence. For the deep QD the energy spacing of the electron states is large enough to suppress the electronic-intersubband contribution of the carrier-phonon dephasing, but the hole-intersubband contributions are still significant. Thus the carrier-phonon dephasing of the quantum coherence is small compared to the carrier-phonon dephasing of the probe polarization. But for the shallow QD the two carrier-phonon dephasing rates are of similar size. The carrier-carrier dephasing rate of the quantum coherence is only slightly different between the deep and the shallow QD. Therefore, compared to the shallow QD, the deep QD has a significantly smaller dephasing rate of the quantum coherence.

Figure 2 shows also the results for the lattice temperature dependence of peak gain and peak slowdown by comparing a lattice temperature of 150 K with a lattice temperature of 300 K for the deep QD. Above a drive intensity of 0.1 MW/cm^2 the peak slowdown factor for similar peak absorption values is higher for lower temperatures. Thus, a slightly enhanced EIT with an improvement of slowdown is obtained for a lattice temperature of 150 K compared to 300 K. The results can be explained in the following way: Because the average phonon occupation is reduced for lower temperatures, a smaller carrier-phonon dephasing rate results for all polarizations. This reduction is more pronounced for the interband and less pronounced for the quantum coherence, which is already small. Additionally, the carrier-carrier dephasing rate exhibits a small, but not significant, change for the quantum coherence between 300 K and 150 K.

Qualitatively, the picture that emerges for group velocity slowdown in single QDs based on a microscopic description of the quantum coherences is the following. The computed group-velocity slowdown of the V-type scheme is considerably larger than that achievable in a Λ-type scheme. In particular, one can obtain group-velocity slowdown with a CW drive field using a realistic model for the sources of dephasing of the quantum coherence. In a Λ scheme, as investigated earlier by us, this is not possible and one needs to resort to pulsed drive fields, which lead to usable slowdown only in a short time window. In the V

configuration investigated here, a deep dot at low temperatures gives the best results, but the carrier-carrier dephasing contributions, while already small, cannot be significantly reduced and therefore set the limit of efficiency for slow light applications. In the next section we show how a reduction of the relevant carrier-phonon and especially *carrier-carrier* contributions to the dephasing can be realized by reducing the overlap of the corresponding wave functions by using suitably designed QD *molecules*.

IV. QUANTUM DOT MOLECULES

In this section we first describe a semi-analytical model to investigate the electronic structure of QD molecules. This approach allows us to specify QD molecule "designs" by the sizes (and material composition) of the individual dots and the distance of the single QDs. For these QD designs we can find, in an approximate way, the associated wave functions and energies. We show how the structural parameters of the QD molecules determine the energy levels and wave functions of the QD molecules. Finally, we choose QD molecule structure optimized for long-lived quantum coherences and calculate the group-velocity slowdown achievable in this structure.

Compared to the single QD model of the last section, we make an adjustment to the confinement potential because an in-plane harmonic oscillator confinement potential has no finite size in plane. If one wants to combine two single dots QDs to a molecule, including the electronic coupling of the single QD states, it is necessary to determine the wave functions and energy levels of the single QDs from a *finite* confinement potential. Since the details of the confinement potential do not decisively affect the final results, it is easier to work with a pillbox model for the single QDs, instead of modifying the harmonic oscillator potential. Starting from the wave functions of this pillbox model for the single QDs, we make an ansatz for the QD molecule states similar to the linear combination of atomic orbitals. As in the QD case, the Coulomb interaction between the electron or hole states is taken into account later in the dynamic calculation using the semiconductor Bloch equations.

A. Electronic structure of a cylindrical QD

We follow here and in the next subsection closely the Appendix in Ref. 31. For the Hamiltonian of the cylindrical QD in envelope approximation we use

$$H = -\frac{\hbar^2}{2m}\nabla^2 + V(r,z) \tag{12}$$

where the Laplacian ∇^2 and the confinement potential

$$V(r,z) = \begin{cases} 0 & \text{for } |z| > a \quad \text{or} \quad |r| > b \\ -V_0 & \text{for } |z| < a \quad \text{and} \quad |r| < b \end{cases} \tag{13}$$

are expressed in cylindrical coordinates. In this approximation, the QD "design" and, consequently, the electronic structure is fixed by the following parameters: the height of the QDs in z direction $h = 2a$, the diameter $2b$, and the depth of the confinement potential V_0. The full envelope wave function Φ_{3D} is the solution of the Schroedinger equation

$$H\Phi_{3\mathrm{D}} = E\Phi_{3\mathrm{D}}. \tag{14}$$

Under the realistic assumption that the height is much smaller than the diameter of the QD, the electrons and holes are strongly localized in the growth direction z. If we assume the separability of the wave function for the in-plane and the z direction, the three dimensional Schroedinger equation can be separated into a 2D and a 1D problem as in Eq. (11). Furthermore we assume, in z direction,

$$\int \Phi_\perp^*(z) V(r,z) \Phi_\perp(z)\, \mathrm{d}z \approx -V_0 \Theta(b - |r|) \tag{15}$$

and the corresponding approximation for the in-plane direction to obtain a self-consistent set of equations.

For the Schroedinger equation in z direction we have

$$\left[-\frac{\hbar^2}{2m}\frac{\partial^2}{\partial z^2} + \tilde{V}_\perp\, \Theta(a - |z|)\right] \Phi_\perp(z) = E_\perp \Phi_\perp(z) \tag{16}$$

Here, $\tilde{V}_\perp = -V_0 + T_\parallel$ is an effective one-dimensional potential that contains the in-plane kinetic energy $T_\parallel = \tilde{V}_\parallel - E_\parallel$ which, in turn, depends on the in-plane eigenenergy $E_\parallel$. Since these kinetic energies $T_\parallel$ are not known, we use an iteration procedure to calculate the in-plane and z eigenenergies. We start the iteration by setting $\tilde{V}_\perp$ equal to $-V_0$. We obtain for the symmetric eigenstates

$$\Phi_{\perp,n}^S(z) = B\Theta(|z| - a)\cos(k_n a) e^{\kappa_n (a - |z|)} + B\Theta(a - |z|)\cos(k_n z) \tag{17}$$

and for the antisymmetric eigenstates

$$\Phi^A_{\perp,n}(z) = C\Theta(|z|-a)\mathrm{sgn}\,(z)\sin(k_n a)e^{\kappa_n(a-|z|)} + C\Theta(a-|z|)\sin(k_n z). \tag{18}$$

Here B and C are normalization constants and we have defined

$$\kappa_n = \frac{\sqrt{2m|E_{\perp,n}|}}{\hbar} \tag{19}$$

$$k_n = \frac{\sqrt{2m\big(|\tilde{V}_\perp| - |E_{\perp,n}|\big)}}{\hbar} \tag{20}$$

The eigenvalues $E_{\perp,n}$ can be determined by the intersection $s_n = k_n a$ of the curves

$$f(ka) = \tan(ka) \tag{21}$$

$$g^S(ka) = \frac{\sqrt{(k_0 a)^2 - (ka)^2}}{(ka)} \tag{22}$$

or

$$g^A(ka) = \frac{-(ka)}{\sqrt{(k_0 a)^2 - (ka)^2}} \tag{23}$$

where $k_0 = \sqrt{2m|\tilde{V}_\perp|/\hbar}$. Finally, the eigenvalues are

$$E_{\perp,n} = \frac{\hbar^2 s_n^2}{2ma^2} - |\tilde{V}_\perp|. \tag{24}$$

For the Schroedinger equation in the in-plane direction we have

$$\Big[-\frac{\hbar^2}{2m}\big[\frac{1}{r}\frac{\partial}{\partial r}\big(r\frac{\partial}{\partial r}\big) + \frac{1}{r^2}\frac{\partial^2}{\partial\varphi^2}\big] + \tilde{V}_\parallel\Theta(b-r)\Big]\Phi_\parallel(r,\varphi) = E_\parallel\Phi_\parallel(r,\varphi) \tag{25}$$

The effective potential $\tilde{V}_\parallel = -V_0 + T_\perp$ again includes a contribution from the kinetic energy in growth-direction, which depends on the solution of the eigenvalue problem in z direction, $T_\perp = \tilde{V}_\perp - E_\perp$. We start the iteration by setting $\tilde{V}_\parallel$ equal to $-V_0$. Because of the symmetry of the potential around the growth direction, the Hamiltonian commutes with the components of the angular momentum operator ($[H, l_z] = 0$). Therefore the two dimensional Schroedinger equation for the angular momentum projection quantum number m_l reduces to an effective one dimensional Schroedinger equation. Resorting the terms we obtain

$$\Big[-\frac{\hbar^2}{2m}\big(\frac{1}{r}\frac{\partial}{\partial r} + \frac{\partial^2}{\partial r^2}\big) + \tilde{V}_\parallel\Theta(b-r) + \frac{\hbar^2}{2m}\frac{m_l^2}{r^2}\Big]\tilde{\Phi}_\parallel(r) = E_\parallel\tilde{\Phi}(r) \tag{26}$$

where

$$\Phi_\parallel(r,\varphi) = \frac{1}{\sqrt{2\pi}}e^{im\varphi}\tilde{\Phi}_{\parallel,m}(\varphi) \tag{27}$$

This equation can be cast into the form of a Bessel differential equation. A solution of this differential equation inside the QD is the Bessel function in m-th order of the first kind $J_m(kr)$, so that we have inside the QD

$$\widetilde{\Phi}_{\parallel,m}(r) = AJ_m(kr) \tag{28}$$

A solution outside the QD is the modified Bessel function $K_m(\kappa_r r)$. Outside the QD we therefore have

$$\widetilde{\Phi}_{\parallel,m}(r) = BK_m(\kappa_r r). \tag{29}$$

At $r = b$, $\Psi'_{\parallel}$ and $\Psi_{\parallel}$ have to be continuous. With $k_0^2 = \frac{2m}{\hbar^2}(-\tilde{V}_{\parallel})$ and $\kappa_{\mathrm{r}} = \sqrt{k_0^2 - k^2}$, the continuity condition yields

$$N(k) = \frac{J'_m(kR)}{J_m(kR)} - \frac{K'_m(\sqrt{k_0^2 - k^2}R)}{K_m(\sqrt{k_0^2 - k^2}R)} = 0 \tag{30}$$

All k_n between 0 and k_0 with $N(k) = 0$ are allowed. For the eigenvalues of the two dimensional problem we obtain

$$E_{\parallel,n} = \frac{\hbar^2 (k_n^2 - k_0^2)}{2m} \tag{31}$$

In summary we have energy levels $E_{\parallel,n,m}$ and wave functions $\Phi_{\parallel,n,m}$ with the quantum numbers n and m. The states with different m and the same n are degenerate.

For the approximate solution of the three dimensional problem we have to solve the one- and two-dimensional eigenvalues in a self-consistent fashion by determining the updated potentials for the next iteration step from the eigen-energies of the previous iteration. The procedure is quite efficient, and one obtains converged eigenvalues $E_{n_z n_r m}$ and wave functions $\Phi_{n_z n_r m}$ for the pillbox-shaped QD after only a few iteration steps. The resulting energies and wave functions, obtained using optimized effective parameters, have been checked against k·p-calculations,[35,36] which include strain and piezoelectric effects.

B. Electronic structure of a QD molecule

We assume that the QD molecules are stacked on top of each other, as can be achieved using vertically correlated growth of QDs.[34] With this method, QDs are grown in layers on top of each other, separated by a spacer layer. For this type of QD molecules we study different QD heights and widths of the spacer layer and analyze the resulting energy spectra and dipole moments.

Using the electronic structure for pillbox shaped QDs, we now couple these QDs to molecules. For this purpose we introduce an ansatz similar to the linear combination of atomic orbitals. We assume a QD molecule consisting of two QDs, labeled 1 and 2. For QD 1 and 2 we assume N and M bound states respectively. Further, for the uncoupled QDs, we label the wave functions Φ_1^n and Φ_2^m, the eigenvalues ε_1^n and ε_2^m and the potential V_a and V_b, respectively. To determine the envelope wave functions Φ, and the corresponding eigenvalues E, of the electronically coupled QDs we use a superposition of the following form

$$\Phi = \sum_n c_1^n \Phi_1^n + \sum_m c_2^m \Phi_2^m \tag{32}$$

With the Hamiltonian

$$\big(H_0 + V_a + V_b\big)\Phi = E\Phi \tag{33}$$

we can apply a multiplication of $(\Phi_1^j)^*$ and a multiplication of $(\Phi_2^k)^*$ respectively. Therefore we obtain in matrix notation

$$\begin{pmatrix} M_1^{jn} & M_2^{jm} \\ M_3^{kn} & M_4^{km} \end{pmatrix} \begin{pmatrix} c_1^n \\ c_2^m \end{pmatrix} = \begin{pmatrix} A_1^{jn} & A_2^{jm} \\ A_3^{kn} & A_4^{km} \end{pmatrix} E \begin{pmatrix} c_1^n \\ c_2^m \end{pmatrix} \tag{34}$$

where

$$M_1^{jn} = \varepsilon_1^n \delta_{jn} + \langle \Phi_1^j | V_b | \Phi_1^n \rangle \tag{35}$$

$$M_2^{jm} = \varepsilon_2^m \langle \Phi_1^j | \Phi_2^m \rangle + \langle \Phi_1^j | V_a | \Phi_2^m \rangle \tag{36}$$

$$M_3^{kn} = \varepsilon_1^n \langle \Phi_2^k | \Phi_1^n \rangle + \langle \Phi_2^k | V_b | \Phi_1^n \rangle \tag{37}$$

$$M_4^{km} = \varepsilon_2^m \delta_{km} + \langle \Phi_2^k | V_a | \Phi_2^m \rangle \tag{38}$$

and $A_1^{jn} = \delta_{jn}$, $A_2^{jm} = \langle \Phi_1^j | \Phi_2^m \rangle$, $A_3^{kn} = \langle \Phi_2^k | \Phi_1^n \rangle$, as well as $A_4^{km} = \delta_{km}$. This generalized eigenvalue problem can be solved numerically with an eigenvalue-solver.[37] Because in this case matrix A is invertible, its possible to reduce the generalized eigenvalue problem to an (ordinary) eigenvalue problem. Therefore we have to solve

$$\left[\begin{pmatrix} A_1^{jn} & A_2^{jm} \\ A_3^{kn} & A_4^{km} \end{pmatrix}^{-1} \begin{pmatrix} M_1^{jn} & M_2^{jm} \\ M_3^{kn} & M_4^{km} \end{pmatrix} \right] \begin{pmatrix} c_1^n \\ c_2^m \end{pmatrix} = E \begin{pmatrix} c_1^n \\ c_2^m \end{pmatrix} \tag{39}$$

The eigenvalues and eigenfunctions of this equation have to be understood as the single-particle result for the electronic structure of the QD molecule, which can then be used as input in the many-particle semiconductor Bloch equations.

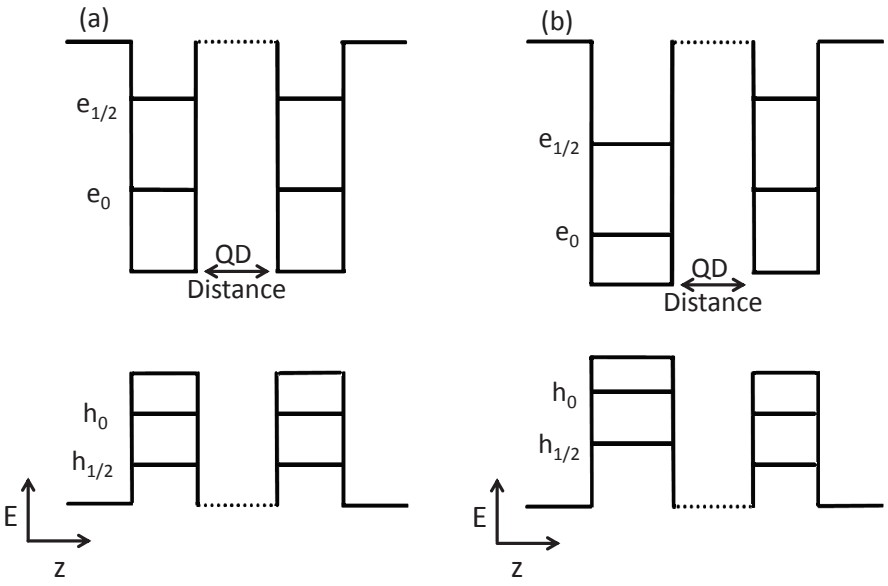

FIG. 3. Schematic picture of the geometry of the symmetric (a) and asymmetric (b) double QD molecules. The QD distance is varied as described in the text.

Furthermore we want to consider an sufficiently weak external electric field, i.e., an electric field that can be included in the LCAO calculation of the QD molecules. For electrons, one includes in the potential $V_a + V_b$ in (33) a contribution from the electric field Fz where F is the electric field. For holes, the sign of the electric potential is reversed. The results of this semi-analytical approach for QD molecules without electric field were again checked against k·p-calculation.[35,36] The approach was found to yield a qualitatively correct description of the electronic structure of the QD molecules studied in this paper.

C. Examples of QD molecules

As shown in figure 3 we assume two cylindrical QDs stacked in z-direction with a QD distance d and an aligned in-plane center of the potential. We will compare the electronic structure and the dipole matrix elements for molecules consisting of identical QDs, e.g., two small QDs, and QDs of different sizes, i.e. a small and a large QD. The parameters used in the semi-analytical model are adjusted to sample QDs calculated using $k \cdot p$-theory. For the sample QD we choose an InAs cylindrical QD embedded in GaAs. We assume for the cylindrical QD a diameter of 16 nm, a height of 3 nm, and call this one the large QD. The

Large Dot			Small Dot		
	E_e (meV)	E_h (meV)		E_e (meV)	E_h (meV)
e/h_0	−192.8	52.0	e/h_0	−144.8	38.8
$e/h_{1/2}$	−105.3	26.6	$e/h_{1/2}$	−62.3	14.9

TABLE II. Electron (e) and hole (h) energies of single-particle states in the single QDs forming the double QD molecules.

input material parameters are taken from Ref. 38. The numerical reference calculation is done by using a single-band approximation for the electron states and a 6×6 k·p-method for the hole states.[35] We find three confined electron and three confined hole states. The energy gap between the electron and the hole ground state of the QD comes out to be 1.2 eV, and the hole ground state is over 90% heavy-hole like. Afterwards, we adjust the parameters and calculate the large QD and the small QD using the semi-analytical approach. For the small QD we assume a diameter of 14 nm and a height of 2.5 nm. The energy eigenvalues of both QDs for our adjusted semi-analytical model are given in table II.

First, we investigate a QD molecule consisting of two identical QDs and use the small QDs for the calculation. We start with a QD distance of 25 nm between the QDs and repeat our calculation with smaller distances until a QD distance of 10 nm is reached. For each distance the wave functions of the QD molecule and the corresponding energy values are determined. The electron and hole energy values for these QD distances are plotted in figure 4. If the distance between the QDs is sufficiently large the bottom and the top dot are electronically decoupled and can be considered as single QDs. Therefore the lowest level and the higher levels of the bottom and top QDs are degenerate. By reducing the distance, the interaction between the QDs becomes stronger, and a bonding and a antibonding state originating from the degenerate states are obtained. As illustrated in figure 5, for identical QDs the bonding state Φ_b can be written as $\Phi_b = \frac{1}{\sqrt{2}}(\Phi_{bt} + \Phi_t)$ and the antibonding state Φ_a can be written as $\Phi_a = \frac{1}{\sqrt{2}}(\Phi_{bt} - \Phi_t)$ over the whole range of possible distances, where Φ_{bt} is the state originating from the bottom and Φ_t is the state originating from the top QD. When the QDs are closer, the interaction becomes stronger and the energy separation between the bonding and antibonding states is larger. For the energetically lower lying states this energy separation is symmetric. For confined states at higher energies the separation is

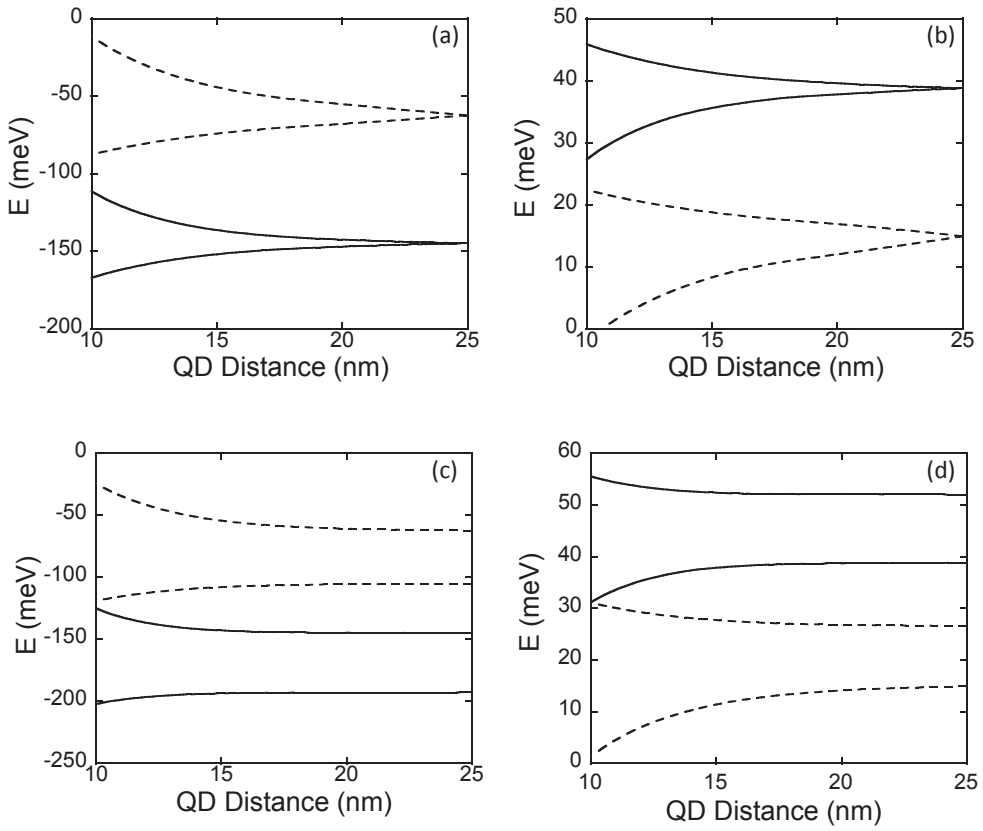

FIG. 4. Energy of the combined conduction (a,c) and valence band states (b,d) plotted over the QD distance between two identical (a,b) and two different sized QDs (c,d) forming a molecule. The solid lines are the bonding and antibonding ground states and the dashed lines are the bonding and antibonding degenerate first and second excited states.

somewhat suppressed for the antibonding state. Qualitatively, the behavior of the bonding and antibonding states over the considered distance range is similar for the conduction and the valence band.

We now turn to QDs of different size. We couple a "bottom" large QD and a "top" small QD. Again we calculate the combined wave functions and the corresponding eigenvalues for several QD distances between 25 nm and 10 nm, and plot the electron and hole energy values in figure 4. If the distance between the QDs is sufficiently large the bottom and the top dot are electronically decoupled and can be considered as single QDs. By reducing the distance the QDs begin to interact with each other and a bonding state originating from the large QD and an antibonding state originating from the small QD is obtained (see figure 4). If the QDs

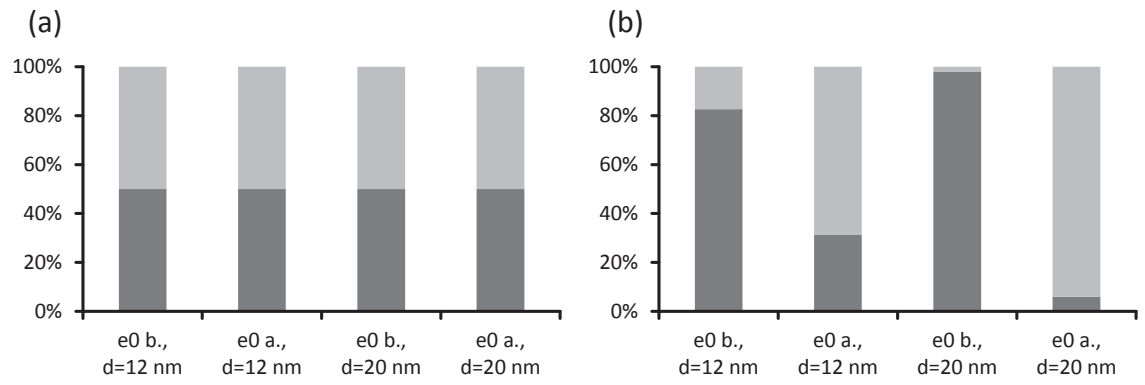

FIG. 5. Composition of the bonding and antibonding ground states for a distance of 12 nm and 20 nm between QDs of identical (a) and different (b) size. The bottom QD is marked black and the top QD is marked grey. In (b) the bottom QD is the "large" QD and the top QD the "small" one.

are closer, the interaction becomes stronger and the energy separation between the bonding and antibonding states is enlarged. In contrast to the identical QDs the composition of the bonding and antibonding states changes with the distance as depicted in figure 5. For shorter distances the bonding states develop an increasing admixture from states originating from the small QD and vice versa. Qualitatively, the behavior of the bonding and antibonding states over the range of distances considered here is again similar for the conduction and the valence band. Generally, comparing Figures 5 (a) and (b) shows that combining QDs of similar size to a molecule will lead to a more efficient mixing of states located at the individual QDs as compared to the combination of QDs with very different sizes.

Finally, the dipole interband and the dipole intersubband matrix elements for the electron states are calculated. For a single QD only diagonal transitions between electron and hole states for the interband matrix elements and the ground state to the first or second excited state for the intersubband matrix elements would be dipole allowed. This behavior carries over to the QD molecule composed of identical QDs, if one regards the bonding and antibonding states as two separate quantum numbers. For the different sized QDs the states become more strongly mixed for decreasing QD distance. An overview of the dipole matrix elements is given in figure 6.

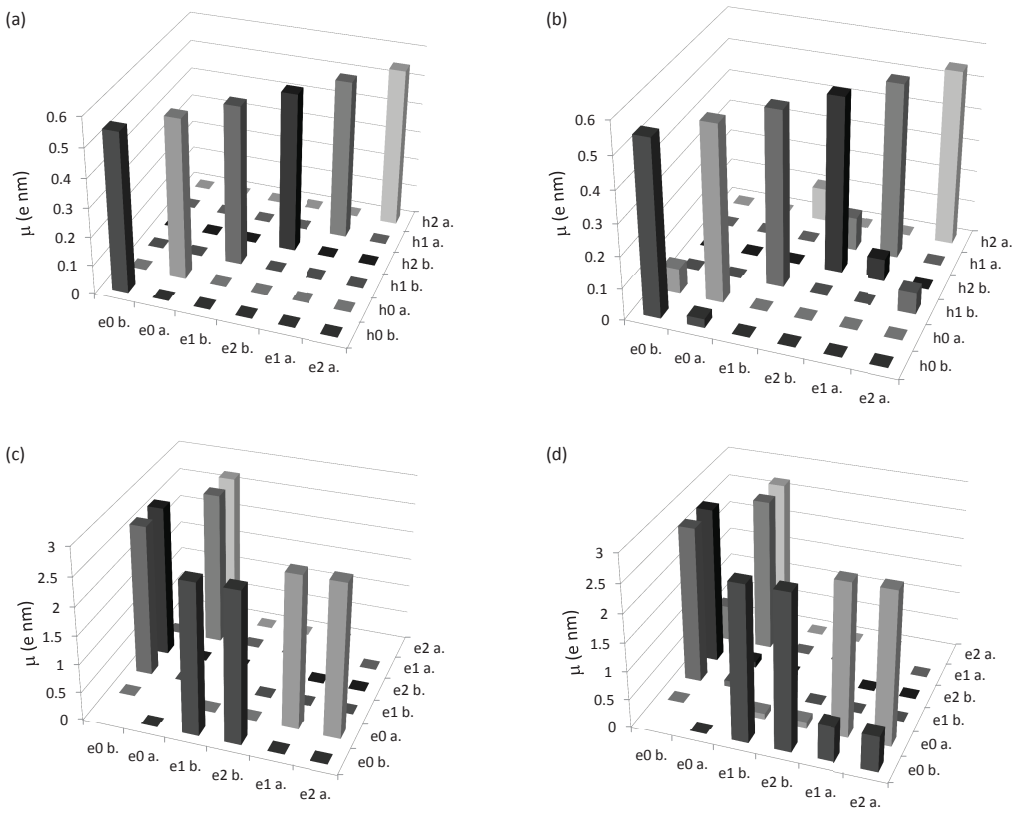

FIG. 6. Dipole interband (a,b) and intersubband (c,d) matrix elements μ for QD molecules consisting of two identical (a,c) and two different sized (b,d) QDs. The bonding and antibonding ground states are labeled e0 b. and e0 a. and the bonding and antibonding degenerate first and second excited states are labeled e1 b., e1 a. and e2 b., e2 a., respectively. The nomenclature for the holes is similar.

D. QD molecule for group-velocity slowdown

The last section showed that QD molecules allow one to tailor the electronic structure by the QD molecule design. The main idea to circumvent the limit of the maximum achievable slowdown in QDs is to design a QD molecule that has spatially well separated electronic wave functions. The spatial separation of the wave functions connected by the quantum coherences minimizes electron phonon and Coulomb matrix elements, which influence the dephasing of this coherence.

First of all, we calculate a small and a large sample QD using $k \cdot p$-theory to adjust the parameters in the semi-analytical model. For both QDs we assume a geometry of an obelisk

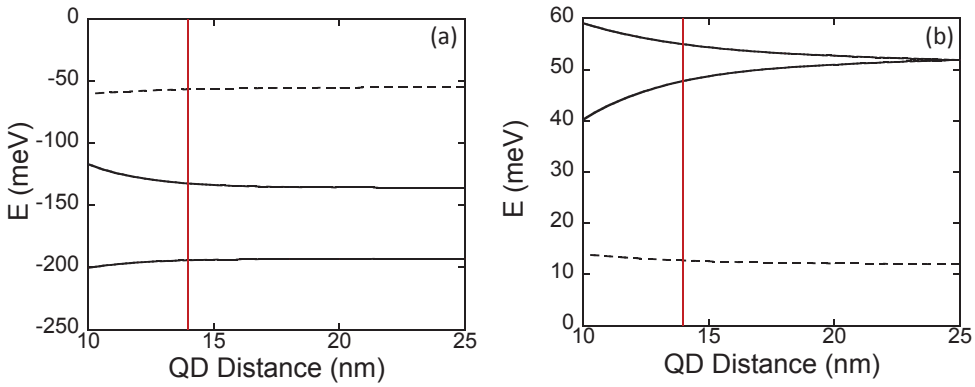

FIG. 7. Combined conduction (a) and valence band states (b) plotted over the distance for the asymmetric double QD molecule described in the text. The solid lines are the bonding and antibonding ground states and the dashed lines are the degenerate first and second excited states.

	E_e (meV)		E_h (meV)
e_0	-194	h_0^b	55
e_1	-132	h_1^a	47
$e_{2/3}$	-56	$h_{2/3}$	13

TABLE III. Electron (e) and hole (h) energies of single-particle states in the QD molecule. The bonding and antibonding states formed from hole levels of the individual QDs are denoted by h^b and h^a, respectively.

with {101} facets. For the small QD geometry we assume an $In_{0.8}Ga_{0.2}As$ QD embedded in a GaAs QW on a wetting layer of thickness 1 nm. The QD has a base of 10 nm × 10 nm and a height of 2 nm. For this configuration only the electron and hole ground states are confined. For the large QD configuration we assume an $In_{0.9}Ga_{0.1}As$ QD embedded in a GaAs QW on a wetting layer of thickness 1 nm. The QD has a base of 12 nm × 12 nm and a height of 3 nm. For this configuration three electron and three hole states are confined. Using the sample QDs we check the parameters in our semi-analytical approach and calculate the electronic structure of the small and the large QD as an intermediary result.

An external electric field in growth direction opens up the possibility to shift the energy levels of the QDs. We choose a field that makes the hole ground states of the small and the large QD degenerate. The other energy levels are not degenerate due to the different

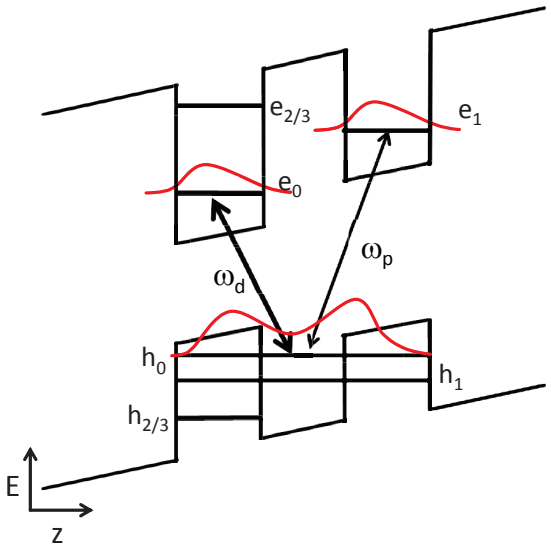

FIG. 8. Schematic picture of the lowest-level wave functions and the geometry of the asymmetric double QD molecule described in the text. The resonant probe and drive fields in a V-type quantum coherence scheme are also shown.

energy spacings of the QDs. If we couple these two QDs including a suitably chosen static electric field in growth direction, we obtain the energy eigenvalues for different QD distances depicted in figure 7. For large distances between the QDs, we have effectively two separate QDs with different energy spacing between the states. Other than between the hole ground states, no degeneracy of an energy level between the small and the large QD occurs. An intermediate QD distance allows one to have bonding and antibonding hole ground states with a sizable energy difference, but without significant mixing with the other states, see figure 7. In particular, the electron ground states of the two QDs are not significantly mixed. This configuration can be realized with a dot distance of 14 nm and a static electric field in growth direction with $E_\perp = 1.5\,\mathrm{mV/nm}$. We have done test calculations for QD molecules which qualitatively confirm the results of our semi-analytical approach. Only the dependence of energy spacing and QD distance is changed somewhat. For instance, a $k \cdot p$-calculation, which includes strain and piezoelectric effects, yields a result of approximately 10 nm for this configuration.[30] The QD molecule with intermediate QD distance is placed in the center of a QW with a thickness of 30 nm. For the QD molecule we obtain four confined hole and electron states. The energy eigenvalues are depicted in figure 8 and compiled in

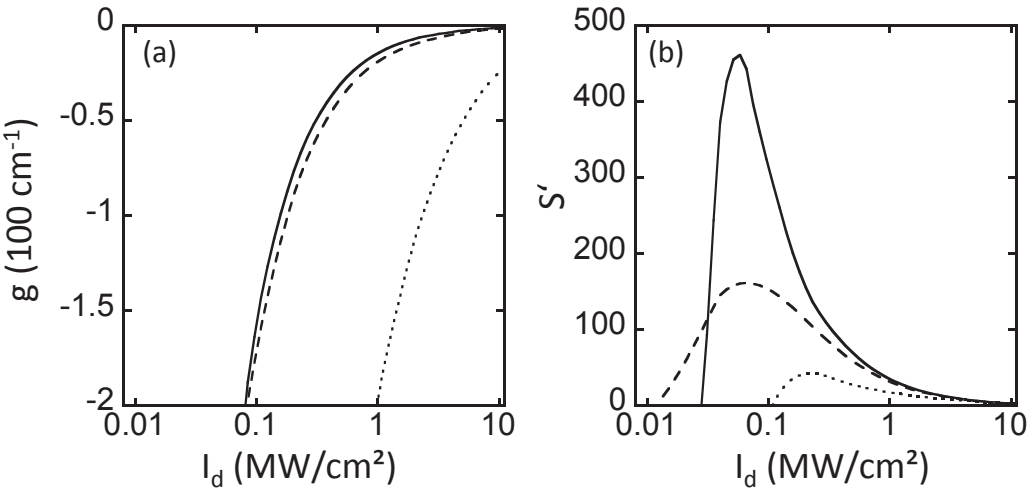

FIG. 9. Peak gain (a) and peak slowdown (b) versus drive intensity for the QD molecule (solid and dashed line) and the deep single QD (dotted line). The lattice temperature is 300 K (dashed line) and 150 K (solid and dotted line).

the table III.

As already mentioned we have a bonding h_0^b and antibonding h_1^a hole ground state and electron ground states $e_{0/1}$ without a significant mixing between the two QDs of the molecule. Therefore the overlap of the wave functions between the two electron ground states is small. The transitions between the bonding hole ground state h_0^b and the electron ground states e_0 and e_1 are dipole allowed with dipole moments of $0.5e$ nm and $0.2e$ nm, respectively. Thus we can realize a V-configuration for the QD molecule as shown in figure 8. The cw drive is chosen resonant with the transition of the bonding hole ground state h_0^b and the electron ground state e_0; the cw probe is chosen resonant to the transition between the bonding hole ground state h_0^b and the electron ground state e_1. The $e_0 \leftrightarrow e_1$ transition is the quantum coherence transition of the V-scheme.

V. QD MOLECULES FOR SLOWING DOWN LIGHT

We use a QD molecule V-scheme as introduced in section IV D for slowing down light and compare the results with the results from the deep single QD. The peak gain and the peak slowdown are calculated as in section III and, as for the single QD, we plot these quantities in figure 9 for different lattice temperatures. As in Section III, we obtain generally a more

efficient slowdown for lower temperatures. The most important result of figure 9 is the comparison of the deep single QD and the QD molecule for a lattice temperature of 150 K. For similar peak absorption values an improvement of the peak slowdown by an order of magnitude for the QD molecule is achieved. This is because in the QD molecule, as compared to the single QD, the dephasing rate of the quantum coherence is much more reduced than the dephasing rate of the interband probe polarization. This reduction comes particularly from the negligible wave-function overlap between the states of the $e_0 \leftrightarrow e_1$ transition. The negligible overlap has a huge influence on the electron-phonon *and electron-electron* dephasing contributions, especially for the quantum coherence. This result demonstrates that suitable QD *molecules* may be extremely effective for engineering long dephasing times in self-organized semiconductor QD systems. Additional numerical results on the behavior of the group-velocity slowdown are contained in Ref. 31.

VI. CONCLUSION

We showed, using a microscopic calculation of scattering and dephasing contributions for the coherences involved, that for group-velocity slowdown in a single QD, a V-type scheme is preferable to a Λ-type scheme. Here, a deep single QD at low temperatures gives the best results. We discussed how a simple model for QDs, which is calibrated by numerical calculations, can be used to analyze the electronic properties of QD *molecules*. In particular, the electronic structure of QD molecules can be designed to lead to a long lived quantum coherence by effectively separating the electronic states of the V system in different QDs while leading to a delocalized bonding hole state. This design minimizes the dephasing of the quantum coherence between the electronic states and leads to a pronounced increase in group-velocity reduction compared to a single QD.

ACKNOWLEDGMENTS

This work was supported in part by Sandia's LDRD program and Energy Frontier Research Center (EFRC) for Solid-State Lighting Science, funded by U.S. Department of Energy, Office of Science, Office of Basic Energy Sciences. WWC thanks the hospitality of the

Technical University Berlin and travel support provided by SFB787.

[1] M. Fleischhauer, A. Imamoglu, and J. P. Marangos, Rev. Mod. Phys. **77**, 633 (2005).

[2] S. E. Harris, J. E. Field, and A. Imamoglu, Phys. Rev. Lett. **64**, 1107 (1990).

[3] M. O. Scully, S. Y. Zhu, and A. Gavrielides, Phys. Rev. Lett. **62**, 2813 (1989).

[4] J. P. Marangos. J. Mod. Opt. **45**, 471 (1998).

[5] J. Mompart, R. Corbalan. J.Opt. B: Quantum Semiclassical Opt. **2**, R7 (2000).

[6] J. Mompart and R. Corbalan, Optics Communications **156**, 133 (1998).

[7] M. Phillips and H. Wang, Phys. Rev. Lett. **89**, 186401 (2002).

[8] A. V. Turukhin, V. S. Sudarshanam, M. S. Shahriar, J. A. Musser, B. S. Ham, P. R. Hemmer, Phys. Rev. Lett. **88**, 023602 (2001).

[9] Z. S. Yang, N. H. Kwong, R. Binder, and A. L. Smirl, J. Opt. Soc. Am. B **22**, 2144 (2005).

[10] S. Sarkar, P. Palinginis, P. C. Ku, C. J. Chang-Hasnain, N. H. Kwong, R. Binder, and H. Wang, Phys. Rev. B **72**, 035343 (2005)

[11] S. W. Chang, S. L. Chuang, P. C. Ku, C. J. Chang-Hasnain, P. Palinginis, and H. L. Wang, Phys. Rev. B **70**, 235333 (2004).

[12] D. D. Smith, H. Chang, K. A. Fuller, A. T. Rosenberger, and R. W. Boyd, Phys. Rev. A **69**, 063804 (2004).

[13] D. E. Nikonov, A. Imamoglu and M. O. Scully, Phys. Rev. B **59**, 12212 (1999).

[14] E. S. Fry, X. Li, D. Nikonov, G. G. Padmabandu, M. O. Scully, A.V. Smith, F. K. Tittel, C. Wang, S. R. Wilkinson, and S.-Y. Zhu, Phys. Rev. Lett. **70**, 3235 (1993).

[15] M. Lindberg and R. Binder, Phys. Rev. Lett. **75**, 1403 (1995).

[16] M.E. Donovan, A. Schülzgen, J. Lee, P. A. Blanche, N. Peyghambarian, G. Khitrova, H. M. Gibbs, I. Rumyatsev, N. H. Kwong, R. Takayama, Z.S. Yang, and R. Binder, Phys. Rev. Lett. **87**, 237402 (2001).

[17] M. Phillips and H. Wang, Opt. Lett. **28**, 831 (2003).

[18] L. V. Hau, S. E. Harris, Z. Dutton, and C. H. Behroozi, Nature (London) **397**, 549 (1999).

[19] D. F. Phillips, A. Fleischhauer, A. Mair, R. L. Walsworth, and M. D. Lukin, Phys. Rev. Lett. **86**, 783 (2001).

[20] P. C. Ku, C. J. Chang-Hasnain, and S.-L. Chuang, Electron. Lett. **38**, 1581 (2002) .

[21] P. Palinginis, S. Crankshaw, F. Sedgwick, E.-T. Kim, M. Moewe, C. J. Chang-Hasnain, H. Wang, and S.-L. Chuang, Appl. Phys. Lett. **87**, 171102 (2005).

[22] K. Kondo, M. Shinkawa,Y. Hamachi,Y. Saito,Y. Arita, and T. Baba, Phys. Rev. Lett. **110**, 053902 (2013).

[23] C. J. Chang-Hasnain, P. C. Ku, J. Kim, and S.-L. Chuang, Proc. IEEE **91**,1884 (2003).

[24] W. W. Chow, H. C. Schneider, and M. C. Phillips, Phys. Rev. A **68**, 053802 (2003).

[25] A. A. Belyanin, F. Capasso, V. V. Kocharovsky, Vl. V. Kocharovsky, and M. O. Scully, Phys. Rev. A **63**, 053803 (2001)

[26] P. Lunnemann and J. Mørk, J. Opt. Soc. Am. B **27**, 2654 (2010).

[27] T. R. Nielsen, A. Lavrinenko, and J. Mørk, Appl. Phys. Lett. **94**, 113111 (2009).

[28] S. Michael, W. W. Chow, and H. C. Schneider, Appl. Phys. Lett. **89**, 181114 (2006).

[29] W. W. Chow, S. Michael, and H. C. Schneider, J. Mod. Opt. **54**, 2413 (2007).

[30] S. Michael, *Theory of Semiconductor Quantum-Dot Systems: Applications to Slow Light and Laser Gain Materials* (Sierke Verlag, Goettingen, 2010)

[31] S. Michael, W. W. Chow, and H. C. Schneider, Phys. Rev. B **88**, 125305 (2013)

[32] H. C. Schneider, W. W. Chow and S. W. Koch, Phys. Rev. B **64**, 115315 (2001).

[33] L. Jacak, P. Hawrylak, A. Wójs, *Quantum Dots*, Springer (1998).

[34] D. Bimberg, M. Grundmann, and N.N. Ledentsov, *Quantum-Dot Heterostructures* (Wiley, Weinheim, 1998)

[35] nextnano^3 code, released: 24-Aug-2004; see www.nextnano.de/nextnano3/.

[36] S. Hackenbuchner, *Elektronische Struktur von Halbleiter-Nanobauelementen im thermodynamischen Nichtgleichgewicht*, Ph. D. thesis, Walter Schottky Institute, TU Munich (2002).

[37] E. Anderson, Z. Bai, C. Bischof, J. Demmel, J. Dongarra, J. Du Croz, A. Greenbaum, S. Hammarling, A. McKenney, S. Ostrouchov, and D. Sorensen, LAPACK Users' Guide. SIAM, Philadelphia, third edition (1999).

[38] I. Vurgaftman, J. R. Meyer, and L. R. Ram-Mohan, J. Appl. Phys. **89**, 5815 (2001)